IEEE Access
Multidisciplinary | Rapid Review | Open Access Journal

Received December 10, 2019, accepted January 10, 2020, date of publication January 21, 2020, date of current version January 29, 2020.

Digital Object Identifier 10.1109/ACCESS.2020.2968421

Trajectory Tracking of Wheeled Mobile Robots Using Z-Number Based Fuzzy Logic

MOHAMED ABDELWAHAB[1], (Member, IEEE), VICTOR PARQUE[2], (Member, IEEE), AHMED M. R. FATH ELBAB[1], A. A. ABOUELSOUD[3], AND SHIGEKI SUGANO[2], (Fellow, IEEE)

[1]Egypt-Japan University of Science and Technology, Alexandria 21934, Egypt
[2]Department of Modern Mechanical Engineering, Waseda University, Tokyo 169-8555, Japan
[3]Electronics and Communication Department, Cairo University, Giza 12613, Egypt

Corresponding author: Victor Parque (parque@aoni.waseda.jp)

This work was supported in part by the JSPS and MOSR-STDF under the Japan-Egypt Research Cooperative Program, and in part by the Japan International Cooperation Agency (JICA) under E-JUST Project.

ABSTRACT Being trajectory tracking key for safe mobile robot navigation, Fuzzy Logic (FL) has been useful in tackling uncertainty and imprecision to realize robust and smooth trajectory tracking. In this paper, we present the Z-number based Fuzzy Logic control for trajectory tracking of differential wheeled mobile robots. The unique point of our approach lies in the ability to encode constraint and reliability in multi-input and multi-output rules, whose antecedent universe considers only the instantaneous measurements of distance and the orientation gaps, and whose consequent universe is computed by the interpolative reasoning and the graded mean integration approach. As a consequence, not only our approach avoids the complexity of encoding error gradients, but also is advantageous to model versatile control rules able to cope with missing observations and noisy inducements on actuators. Our experiments using both physics-based simulations and real-world tests based on a Pioneer 3DX robot architecture have elucidated the superior efficacy and the feasibility of the proposed controller regarding accuracy, robustness, and smoothness compared to other well-known related frameworks such as Fuzzy Logic Type 1, Fuzzy Logic Type 2 and Fuzzy Logic with PID. Our results provide unique insights to realize generalizable algorithms aided by FL and Z-number towards robust trajectory tracking.

INDEX TERMS Trajectory tracking, mobile robot, fuzzy logic, interpolative reasoning, Z-number.

I. INTRODUCTION

The recent spread of technological advancements have led mobile robots into the increasingly influential role throughout business segments facing cutting-edge innovation, rising costs and deficit in labor, such us autonomous vehicles, agriculture, forestry, manufacturing, exploration and transportation [1], [2]. In line of the above, since the pure pursuit strategy proposed by Wallace et al. in the mid 80's [3], the trajectory tracking problem has attracted the attention of the robotics community and has motivated the development of high-order and versatile motion planning and control algorithms. The reader may refer to [4] for a review on the developments of pure pursuit and the related approaches.

Although the pure pursuit strategy is a straightforward, simple and widely known controller in trajectory tracking, it is well-understood that tuning of the (look-ahead) radius parameter is essential to realize smooth robot trajectories with the concomitant requirement for high accuracy. Conversely, having habitually emerged in the Robotics, Control and Machine Learning communities, the self-tuning learners, such as the Fuzzy-PID, PID with Neural Networks and PID with Genetic Algorithms, and the related non-linear adaptive control algorithms, such as the adaptive PID with minimum variance [5], allow control algorithms to perform well in changing environments and a variety of scenarios, aiming at smoothness of trajectories and comfortability of drive.

Notwithstanding early trajectory tracking approaches were inspired by single-input-single-output control systems, such as PID, researchers proposed more amenable and flexible schemes able to model the multi-input-multi-output complexity of mobile robots, such as Model Predictive Control (MPC) and Linear Quadratic Regulators (LQR). As such, one of the recent developments concerns the tracking error

The associate editor coordinating the review of this manuscript and approving it for publication was Amjad Ali.

learning control for path tracking of mobile robots in outdoor environments proposed in [6], in which the method tackles the mismatch between the dynamics of the plant and the model to update the control actions, reducing the euclidean error despite high level of noise compared to the conventional error-based control method. Also, the MPC with robot dynamics and the lateral slip of tires was developed in [2], [7], in which simulations show the improved accuracy and the decrease of errors in displacement, heading and lateral velocity compared to the model based on kinematics. MPC with an active safety steering control unit was developed by Junyu Cai et al. [8], showing the control efficacy and the vehicle comfortability due to minimal lateral acceleration and rollover stability.

Other forms of adaptation in trajectory tracking based on recursive methods and observers were also proposed in the literature. By using an augmented vehicle model considering both kinematic and dynamic equations of motion, a back-stepping controller was addressed in [9] achieving exponential convergence to the followed trajectory; yet uncertainties, saturation and actuator failures during motion were unaddressed topics. By using a three-order dynamic system, the adaptive sliding mode trajectory tracking with external disturbances and inertia uncertainties was proposed in [10], in which results show the robustness being able to eliminate external forces and inertia uncertainties. Muhammad Asif et al. [11] developed the output feedback with adaptive Sliding Mode Controller (SMC), and revealed that the high gain observer and the globally bounded state feedback is robust against un-modeled dynamics and disturbances. In [12], the Vector-Field-Orientation (VFO) control was proposed to solve the path following task for unicycle kinematics with the amplitude-limited control input. This method has advantages such as rapid, non-oscillatory, and easily predictable transients in the closed-loop system. Ren and Ma [13] designed the trajectory tracking control for an omnidirectional mobile robot, showing that a state observer estimating unknown internal dynamics and external disturbances compensated the friction effects effectively and improved the accuracy in tracking. Path following using a nonlinear Lyapunov-based control law considering a bounded curvature and nonholonomic constraints of a skid-steered mobile robot was presented by Huskic et al. [14]; here, experiments show reduction in the mean error at higher speeds on various types of terrain. In [15], a model-based adaptive observer was used to estimate the sliding effect and the cornering stiffness of tires, and to determine the steering angle by backstepping-adaptive control, showing reduction in the mean and the maximum absolute error at low and medium speed in off-road contexts.

Conventional controllers based on PID and MPC depend on the accurate estimation of the controller coefficients of the system model. In contrast, Fuzzy Logic (FL) is well-known to be independent on the system model, yet the performance relies on the versatility to handle uncertain and imprecise information. For instance, Fuzzy Logic Type-1 was shown to handle imprecision to a controllable degree in tuning PID gains [16], [17]. Wu et al. [18] presented the trajectory tracking control based on kinematic back-stepping and Fuzzy Sliding Mode, in which numerical results exhibited the improved accuracy, rapidity and smoothness compared to the conventional Sliding Mode Control (SMC). Seongsoo et al. [19] used the Artificial Immune method to optimize the output scaling coefficient of Fuzzy Logic and to improve the overall tracking error. Dian et al. [20] developed the Type-2 Fuzzy Logic to adjust the gains of SMC-based trajectory tracking, achieving decreased tracking error and improved response time under random external disturbances in x and y-axis compared to the non-singular terminal SMC with and without FL. Wu et al. [21] developed the SMC with FL able to generate virtual reference inputs and a function approximation of robot dynamics based on Fourier-series, being more robust compared to PID considering uncertainties, unknown dynamics, saturated control inputs and external disturbances.

In 2011, L. Zadeh showed that the reliabilities of linguistic terms are significant to extend the versatility of reasoning using Fuzzy variables [22]. Here, the concept of a Z-number was proposed as a 2-tuple, in which the first component represents the constraints and uncertain information, and the second component encodes the reliability and confidence of truth. Nowadays, Z-number is being actively used to solve multidisciplinary decision making problems [23]–[27]. Aliev et al. [28] proposed Z-number based Fuzzy system for the Multi-Criteria Decision-Making (MCDM), and Kang et al. [29] proposed the method to convert Z-number to Fuzzy number. And, in [30], an omnidirectional robot was shown to navigate effectively by using Z-number based FL, in which the controller is able to reach a number of waypoints in the plane under carefully fixed steering angles.

Although Z-numbers have attracted the attention of the Control and Robotics community, it is unclear whether Z-numbers are effective in multi-input-multi-output trajectory tracking control schemes when the gradient of the tracking errors are unknown, and whether competitive performance is attainable in challenging and curvature-varying trajectory tracking scenarios. Thus, in this paper, to answer these questions, our contributions are as follows:

- We present a Z-number based Fuzzy Logic (Z-FL) trajectory tracking control scheme with rules modeling the multi-input and multi-output nature of mobile robots. Our approach is inspired by the study of [30]; however, unlike [30], our scheme encodes the control rules only based on instantaneous measurements of distance to target and orientation gaps, which is more amenable to model control rules with finer and non-linear landscape, and more amenable to evaluate and to adapt the performance at high resolution, being relevant for practical navigation scenarios. Also, unlike [30], our approach avoids using the gradient of the tracking errors, which is due to our aim in evaluating the performance frontiers of our approach to navigate in scenarios with varying curvature. The consequent universe is computed

by the interpolative reasoning based on α-cuts [31], and defuzzification is performed by the graded mean integration representation [32]. Whereas the interpolative reasoning enables to tackle missing observations in the extended rule base, the inference system preserves much of the information while performing Fuzzy operations. As a result, our approach is advantageous to encode not only constraints, but also the reliability of sophisticated rules, extending the versatility in modeling the control landscape.

- To validate the efficacy and the robustness of the proposed controller, (1) we performed rigorous computational and real-world experiments using a physics-based simulation environment and a Pioneer 3DX mobile robot, (2) we evaluated the trajectory tracking performance not only by using relevant considerations on accuracy, but also using trajectories with distinct curvature profiles and diverse levels of disturbance, and (3) we compared to the existing well-known frameworks based on Fuzzy Logic (FL): FL-Type 1, FL-Type 2 and FL with PID.
- Our results demonstrate that our approach brings the overall improved performance in terms on accuracy, robustness and smoothness compared to the existing well-known frameworks relevant to trajectory tracking based on Fuzzy-Logic, and provides unique insights useful to realize control algorithms towards robust and generalizable trajectory tracking performance.

The rest of this paper is organized as follows: Section II presents the preliminary concepts; Section III describes the trajectory tracking using Z-number based Fuzzy Logic. In Section IV, simulation studies and results are discussed, and Section V presents the insights on real-world tests. Section VI concludes this paper.

II. PRELIMINARIES

In this section, we describe the fundamental ideas related to our approach.

A. MOBILE ROBOT KINEMATICS

We consider a differential wheeled mobile robot consisting of a structure with two driving wheels mounted on the front axle, and one caster wheel on the rear axle. The kinematic equation of such configuration is as follows:

$$\begin{bmatrix} \dot{X}(t) \\ \dot{Y}(t) \\ \dot{\phi}(t) \end{bmatrix} = \begin{bmatrix} v \cdot \cos\phi \\ v \cdot \sin\phi \\ \omega, \end{bmatrix} \tag{1}$$

where v and ω are linear and angular velocities of the robot (Fig. 1), and ϕ is the heading direction. Linear and angular velocities are defined as follows:

$$\begin{bmatrix} v \\ \omega \end{bmatrix} = \begin{bmatrix} (\omega_r + \omega_l) r_\omega / 2 \\ (\omega_r - \omega_l) r_\omega / L, \end{bmatrix} \tag{2}$$

where ω_r (ω_l) is the angular velocity of the right (left) wheel, r_ω is the wheel radius, and L is the distance between the frontal wheels.

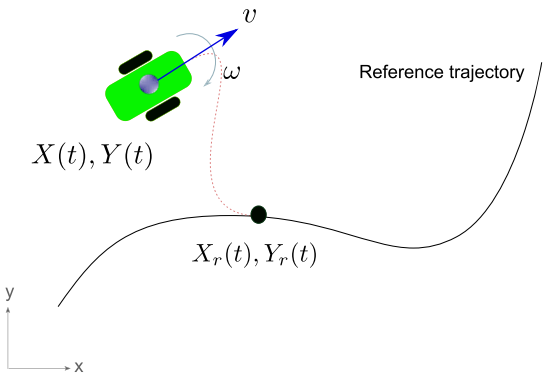

FIGURE 1. Basic idea of trajectory tracking in a differential drive mobile robot.

Basically, the above-described model is under-driven due to two degrees of freedom and three variables. Therefore, only two variables can be actively tracked, and the remaining one is a follow-up state. The errors of position and orientation in the global system at time t are defined as follows:

$$\begin{bmatrix} X_e(t) \\ Y_e(t) \\ \phi_e(t) \end{bmatrix} = \begin{bmatrix} X_r(t) - X(t) \\ Y_r(t) - Y(t) \\ \phi_r(t) - \phi(t), \end{bmatrix} \tag{3}$$

where $X_r(t)$ and $Y_r(t)$ denote coordinates of the reference trajectory along the X-axis and the Y-axis, respectively, and $\phi_r(t)$ is the reference angle.

B. FUZZY LOGIC CONTROL (FLC)

In a FLC system with m inputs, a Fuzzy System (FS) A_j ($j \in [m]$) is defined as follows:

$$A_j = \Big\{ (x_j, \mu_A(x_j)) \mid \mu_A(x_j) \in [0, 1] \; \forall x_j \in \mathbb{R} \Big\}, \tag{4}$$

where $\mu_A : x_j \to [0, 1]$ is the membership function, whose representation using a convex triangular shape is as follows:

$$\mu_A(x_j) = \begin{cases} 0, & \text{if } x_j < a_1 \\ \mathcal{L} = \left(\dfrac{x_j - a_1}{a_2 - a_1}\right), & \text{if } x_j \in [a_1,\ a_2] \\ \mathcal{R} = \left(\dfrac{a_2 - x_j}{a_3 - a_2}\right), & \text{if } x_j \in [a_2,\ a_3] \\ 0, & \text{if } x_j > a_3, \end{cases} \tag{5}$$

where $a_1 \le a_2 \le a_3$ as shown by Fig. 2-(a), and $\mathcal{L}(\mathcal{R})$ is a strictly increasing (decreasing) function in the given interval. Then, in a set with n rules, and $\mathbf{x} \in \mathbb{R}^2$, $\mathbf{x} = (x_1,\ x_2)$, the ith rule is:

$$\lambda_i : \text{If } x_1 \text{ is } A_{i,1} \ \wedge \ x_2 \text{ is } A_{i,2} \ \to \ \varphi \text{ is } B_i, \tag{6}$$

where B_i is a consequent FS, $x_1 = e$ and $x_2 = \dot{e}$. Thus, a Fuzzy mapping in FLC is a function $\varphi : \mathbf{x} \to \mathbb{R}$, as shown by Fig. 2 (b). A typical mapping is defined by the centroid

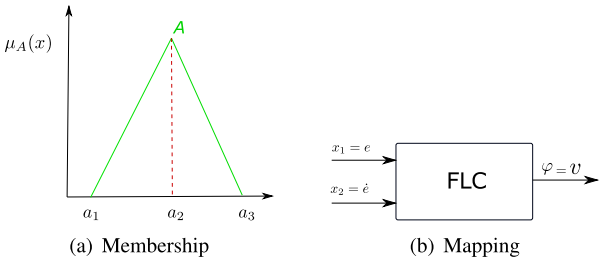

(a) Membership (b) Mapping

FIGURE 2. **(a) Basic concept of a triangular membership function. (b) Basic concept of mapping in FLC.**

defuzzification:

$$\varphi(\mathbf{x}) = \frac{\sum_{i=1}^{n} f_i(\mathbf{x}) \cdot B_i}{\sum_{i=1}^{n} f_i(\mathbf{x})}, \tag{7}$$

$$f_i(\mathbf{x}) = \mu_{A_{i,1}}(x_1) \cdot \mu_{A_{i,2}}(x_2), \tag{8}$$

where φ denotes the control signal v, and $f_i(\mathbf{x})$ denotes the firing strength of the ith rule for observation $\mathbf{x}$ computed from the product t-norm of membership functions ($i \in [n]$).

III. TRAJECTORY TRACKING USING Z-NUMBER BASED FUZZY LOGIC

In this section, we describe Z-number-based Fuzzy Control (Z-FL) for trajectory tracking.

A. BASIC CONCEPT

The control architecture is shown by Fig. 3, whose basic idea is to realize the control mapping Z-FL : $(D(t), \phi_e(t)) \rightarrow (v(t), \omega(t))$ by using the (given) reference trajectory $(X_r(t), Y_r(t))$ and both the position $X(t), Y(t)$ and the heading direction $\phi(t) \in [-\pi, \pi]$ at time t. In Fig. 3, the block DH computes the following:

$$D(t) = \left\| \mathbf{p_e}(t) \right\|, \tag{9}$$

$$\phi_e(t) = \text{sgn}(q_z) \cdot \arccos\left(\frac{\hat{\mathbf{u}}_\phi(t) \cdot \mathbf{p_e}(t)}{D(t)} \right), \tag{10}$$

where $\| \cdot \|$ denotes the Euclidean norm, the vector $\mathbf{p_e}(t) = (X_e(t), Y_e(t), 0)$ denotes the error of the position at time t, $\phi_e(t) \in [-180°, 180°]$ denotes the error in the heading direction, sgn$(\cdot)$ denotes the signum function, q_z is the z-component of the vector $\mathbf{q} = \hat{\mathbf{u}}_\phi(t) \times \mathbf{p_e}(t)$, arccos$(\cdot)$ denotes the inverse cosine ($\cos^{-1}$) in degrees, and $\hat{\mathbf{u}}_\phi(t) = (\cos\phi(t), \sin\phi(t), 0)$ is the unitary vector of the heading direction at time t. The reader may note that both vectors $\mathbf{p_e}(t)$ and $\hat{\mathbf{u}}_\phi(t)$ are defined in the xy-plane, and that the range of $\phi_e(t) \in [-180°, 180°]$ is defined as such due to sgn$(\cdot) = \{-1, 0, +1\}$ and $0° \leq \arccos(\cdot) \leq 180°$.

The architecture portrayed by Fig. 3 is advantageous since it allows a single Z-FL function to map error to control signals of linear and angular velocity. Such concept enables not only the unified interface to model sophisticated rules for robot control, but also the simple and computationally-efficient framework. Furthermore, the ability to include input gradients, orientation references, environment conditions and user preferences becomes straightforward. Yet the study of Z-FL structures with increased sophistication is out of the scope of this paper and left for future studies in our agenda.

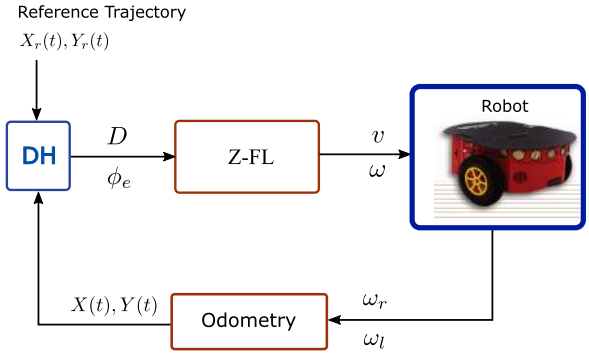

FIGURE 3. **Control architecture for trajectory tracking.**

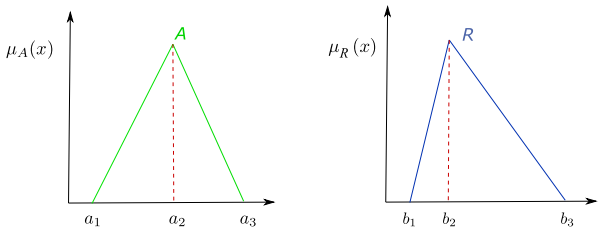

(a) Constraint (b) Reliability

FIGURE 4. **Basic concept of a Z-number, $Z = (A, R)$. The first component denotes the (a) Constraint A, and the second one denotes the (b) Reliability R.**

B. Z-NUMBER

In Z-FL, a Z-number [22] is an ordered tuple:

$$Z_j = \left\{ (A_j, R_j) \mid \mu_{A_j} \in [0, 1],\ \mu_{R_j} \in [0, 1] \right\}, \tag{11}$$

where $j \in [m]$, m denotes the number of inputs, A_j is the constraint (restriction) on the values of observation $\mathbf{x}$, and R_j is the reliability metric (or degree of truth) of A_j. For reasons of simplicity in modeling and efficiency in computation, A and R are defined by triangular MFs (Eq. 5), as exemplified by Fig. 4.

C. INTERPOLATIVE REASONING

In a set of n Z-FL rules and m inputs, the ith rule is expressed as follows:

$$\lambda_i : \text{If } x_1 \text{ is } Z_{i,1} \ \wedge\ x_2 \text{ is } Z_{i,2} \ldots x_m \text{ is } Z_{i,m} \rightarrow \varphi \text{ is } Z_i^C, \tag{12}$$

where $Z_{i,j} = (A_{i,j}, R_{i,j})$ denotes the Z-number for the ith rule ($i \in [n]$) and the jth input ($j \in [m]$), and $Z_i^C = (B_i, R_i)$ is a consequent Z-number.

In the context of trajectory tracking of a mobile robot, $x_1 = D(t)$ and $x_2 = \phi_e(t)$ (outlined in Fig. 3) represent the antecedent universe modeled by triangular MFs, as shown

TABLE 1. Rules for trajectory tracking.

$D(t)$ / ϕ_e	OFF,U		TVVN,U		VVN,U		VN,U		N,U		F,U		VF,U		VVF,U		TVF,U	
	v	ω	v	ω	v	ω	v	ω	v	ω	v	ω	v	ω	v	ω	v	ω
TVLN,U	O,U	N,U	O,U	N,U	O,U	N,U	O,U	N,U	O,U	N,U	O,U	N,U	O,U	N,U	O,U	N,U	O,U	N,U
VVLN,U	O,U	N,U	O, U	N,U	O,U	N,U	O,U	N,U	O,U	N,U	O,U	N,U	O,U	N,U	O,U	N,U	O,U	N,U
VLN,U	O,U	N,U	O,U	N,U	O,U	N,U	O,U	N,U	O,U	N,U	O,U	N,U	O,U	N,U	O,U	N,U	O,U	N,U
LN,U	O,U	N,U	O,U	N,U	O,U	N,U	O,U	N,U	O,U	N,U	O,U	N,U	O,U	N,U	O,U	N,U	O,U	N,U
SN,U	O,U	N,U	O,U	N,U	O,U	N,U	O,U	N,U	O,U	N,U	O,U	N,U	O,U	N,U	O,U	N,U	O,U	N,U
VSN,U	O,U	N,U	O,U	N,U	O,U	N,U	O,U	N,U	O,U	N,U	O,U	N,U	O,U	N,U	O,U	N,U	O,U	N,U
VVSN,U	O,U	SN,U	O,U	SN,U	O,U	SN,U	O,U	SN,U	O,U	SN,U	O,U	SN,U	O,U	SN,U	O,U	SN,U	O,U	SN,U
TVSN,U	O,U	SN,U	O,U	SN,U	O,U	SN,U	O,U	SN,U	O,U	SN,U	O,U	SN,U	O,U	SN,U	O,U	SN,U	O,U	SN,U
OFF,U	O,U	O,U	SL,U	O,U	F,U	O,U	F,U	O,U	F,U	O,U	F,U	O,U	F,U	O,U	F,U	O,U	F,U	O,U
TVSP,U	O,U	SP,U	O,U	SP,U	O,U	SP,U	O,U	SP,U	O,U	SP,U	O,U	SP,U	O,U	SP,U	O,U	SP,U	O,U	SP,U
VVSP,U	O,U	SP,U	O,U	SP,U	O,U	SP,U	O,U	SP,U	O,U	SP,U	O,U	SP,U	O,U	SP,U	O,U	SP,U	O,U	SP,U
VSP,U	O,U	P,U	O,U	P,U	O,U	P,U	O,U	P,U	O,U	P,U	O,U	P,U	O,U	P,U	O,U	P,U	O,U	P,U
SP,U	O,U	P,U	O,U	P,U	O,U	P,U	O,U	P,U	O,U	P,U	O,U	P,U	O,U	P,U	O,U	P,U	O,U	P,U
LP,U	O,U	P,U	O,U	P,U	O,U	P,U	O,U	P,U	O,U	P,U	O,U	P,U	O,U	P,U	O,U	P,U	O,U	P,U
VLP,U	O,U	P,U	O,U	P,U	O,U	P,U	O,U	P,U	O,U	P,U	O,U	P,U	O,U	P,U	O,U	P,U	O,U	P,U
VVLP,U	O,U	P,U	O,U	P,U	O,U	P,U	O,U	P,U	O,U	P,U	O,U	P,U	O,U	P,U	O,U	P,U	O,U	P,U
TVLP,U	O,U	P,U	O,U	P,U	O,U	P,U	O,U	P,U	O,U	P,U	O,U	P,U	O,U	P,U	O,U	P,U	O,U	P,U

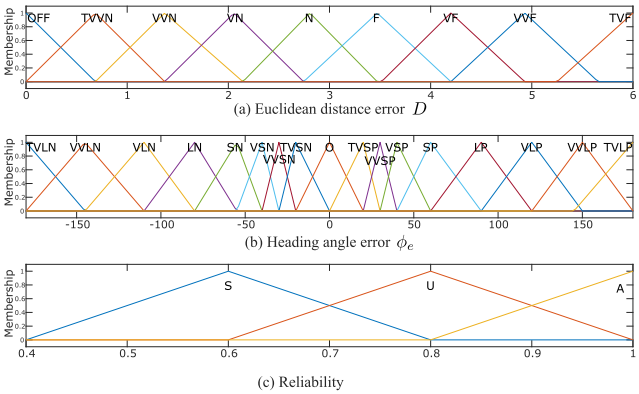

FIGURE 5. Membership functions of (a and b) the antecedent *D* and ϕ_e, and (c) the reliability metric.

by Fig. 5 (a)-(b), and the consequent universe consists of the linear velocity $\varphi_1 = v(t)$ and the angular velocity $\varphi_2 = \omega(t)$ as high-level control signals (outlined by Fig. 3 and defined by the rule set in Table 1). The linguistic values for distance D are: OFF Range (OFF), Too Very Very Near (TVVN), Very Very Near (VVN), Very Near (VN), Near (N), Far (F), Very Far (VF), Very Very Far (VVF), Too Very Far (TVF). And the linguistic values for the heading angle error ϕ_e are: Too Very Large Negative (TVLN), Very Very Large Negative (VVLN), Very Large Negative (VLN), Large Negative (LN), Small Negative (SN), Very Small Negative (VSN), Very Very Small Negative (VVSN), Too Very Small Negative (TVSN), Zero (OFF), Too Very Large Positive (TVLP), Very Very Large Positive (VVLP), Very Large Positive (VLP), Large Positive (LP), Small Positive (SP), Very Small Positive (VSP), Very Very Small Positive (VVSP), Too Very Small Positive (TVSP). The reliability terms for both the antecedent and consequent are defined over Sometimes (S), Usually (U), and Always (A), as shown by Fig. 5 (c). Compared to the conventional approaches, the large number of instances in Table 1 allow not only to define control rules with finer granularity [33], but also allows to adapt the performance of Z-FL with the response at high resolution, being relevant for practical navigation scenarios.

Thus, when observation $\mathbf{x} = (x_1, x_2, ..., x_m)$ is known, with $x_j = Z_j^* = (A_j^*, R_j^*)$, $j \in [m]$, each Z-number $\varphi^*(\mathbf{x}) = (B^*, R^*)$ in the consequent universe is computed as follows:

$$\varphi^*(\mathbf{x}) = \frac{\sum_{i=1}^{n} f_i(\mathbf{x}) \cdot (B_i^\alpha, R_i^\alpha)}{\sum_{i=1}^{n} f_i(\mathbf{x})} \tag{13}$$

$$f_i(\mathbf{x}) = \frac{1}{d_i^\alpha(\mathbf{x}, A^*) + d_i^\alpha(\mathbf{x}, R^*)}, \tag{14}$$

where $\varphi^* : \mathbf{x} \to (B^*, R^*)$ denotes the α-cut interpolation function [31], B_i^α denotes the α-cut of the consequent of the ith rule, and $d_i^\alpha(\mathbf{x}, A^*)$ denotes the distance between the observation $\mathbf{x}$ and A^* w.r.t. the ith rule and overall inputs $j \in [m]$ based on the α-cut interpolation [26], [31], [34]. Here, $\alpha = 0$ corresponds to the lower level of the triangular MFs, while $\alpha = 1$ corresponds to the mid-point of the triangular MFs. In the above description, the consequent $\varphi^*(\mathbf{x}) = (B^*, R^*)$ is the result of a weighted average of the set of antecedent rules, in which rules with smaller distance (implying high similarity) to the observation $\mathbf{x} \sim Z^* = (A^*, R^*)$ receive higher weighting importance. Compared to the conventional approaches, the interpolative mechanism is useful to enhance the robustness of reasoning over sparse rules, enabling the deduction of consequents in situations in which the observation is unable to match missing antecedents.

D. INFERENCE SYSTEM

Defuzzification of the above-computed consequent Z-number $\varphi^*(\mathbf{x}) = (B^*, R^*)$ is realized by the canonical representation of the multiplication of triangular Fuzzy numbers [32], as follows:

$$\varphi(\mathbf{x}) = P(B^*) \cdot P(R^*), \tag{15}$$

where $\varphi : \varphi^*(\mathbf{x}) \to \mathbb{R}$ denotes a mapping from the Z number $\varphi^*(\mathbf{x}) = (B^*, R^*)$ to a crisp value, and $P(\cdot)$ denotes the Graded Mean Integration Representation (GMIR) of a Fuzzy number

[35], defined as follows:

$$P(A) = \frac{\int_0^{w_A} \frac{h}{2}(\mathcal{L}^{-1} + \mathcal{R}^{-1})}{\int_0^{w_A} h \cdot dh}, \tag{16}$$

where A is a Fuzzy number, $w_A \in [0, 1]$, $h \in [0, 1]$, and $\mathcal{L}^{-1}$ is the inverse of function $\mathcal{L}$ (Eq. 5).

When the Fuzzy number A is defined by a triangular MF with the tuple (a_1, a_2, a_3) (Eq. 5), the following holds [32], [36]:

$$P(A) = \frac{a_1 + 4a_2 + a_3}{6} \tag{17}$$

The above-described defuzzification allows to compute with Fuzzy numbers efficiently while preserving much of the information in the embedded ambiguity, and enables efficient canonical Fuzzy operations such as addition, multiplication and ranking [32], [36], [37].

E. PERFORMANCE CRITERIA

In order to evaluate the effectiveness of trajectory tracking, a number of relevant performance indexes are used, as follows:

- Integral of the Absolute Error: IAE_{xy} and IAE_D which denote the accumulated error from the set-point over time and which is suitable for small settling time [13].

$$\text{IAE}_{xy} = \int_0^T \Big(|X_e(t)| + |Y_e(t)|\Big) dt \tag{18}$$

$$\text{IAE}_D = \int_0^T D(t) dt \tag{19}$$

- Maximum Absolute Error (MAE_{xy}) [13] and Maximum Error ($\max_D$) which is useful to judge the suitability for narrow environments.

$$\text{MAE}_{xy} = \max \left\{ \max_{t\in[0,T]} X_e(t), \max_{t\in[0,T]} Y_e(t) \right\} \tag{20}$$

$$\max_D = \max_{t\in[0,T]} D(t) \tag{21}$$

- Root Mean Square Error ($RMSE_D$) [38] which is useful to evaluate the occurrence of large errors.

$$\text{RMSE}_D = \sqrt{\frac{1}{H} \int_0^T \Big[D(t)\Big]^2 dt}, \tag{22}$$

where $|\cdot|$ denotes absolute value, and H denotes the number of measurements for trajectory tracking overall the time interval $t \in [0, T]$. For simplicity and without loss of generality, $H = 1 + T/h$ for small h which is set according to hardware (robot) and software considerations (described in next Sections).

IV. SIMULATION STUDIES

To evaluate the effectiveness and the feasibility of the Z-FL control for trajectory tracking within the context of a differential wheeled mobile robot, we performed rigorous computational experiments. This section describes our configurations and presents our key findings.

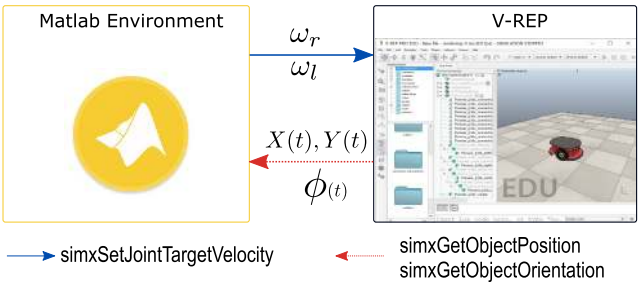

FIGURE 6. Matlab and Pioneer P3-DX mobile robot in V-REP.

A. SIMULATION SETTINGS

We implemented the model of the differential wheeled mobile robot described in Section (2), and its trajectory tracking using Z-FL control strategy described in Section (3) using Matlab 2018(b) and V-REP. The model in V-REP is based on a physics-based Pioneer 3DX mobile robot, which is a differential mobile robot with two frontal driver wheels, a rear caster wheel (driven) and 16 ultrasonic sensors.

In V-REP, we used the bullet physics engine (v.2.78) with simulation mode at accurate (default) level and time step 50 *ms*. The Matlab environment communicates with V-REP by the legacy remote API which supports blocking calls and bidirectional data streaming, as portrayed by Fig. 6.

Our computing environment was an Intel(R) Xeon(R) Gold 6140 CPU @2.3GHz, 128 GB RAM, 16 cores, 32 threads and Windows 10, 64 bit. The sophistication on both Fuzzy rule composition and mobile robot modeling (e.g. addition of sensors) brings no significant difference on the measurement of performance due to (1) the large pool of cores/threads available for computation, and (2) the reasonable amount of available memory to store measurements.

In order to evaluate and compare the trajectory tracking performance to the approaches being relevant to our scope, we implemented and contrasted to trajectory tracking schemes based on FL. In particular, we compared the performance of Z-FL against the following: (1) FL-Type 1 [39] (for simplicity, we will refer to it as FL), (2) FL-Type 2 [40] and (3) FL-PID [16], [17].

To ensure fairness in our comparisons, the rule bases for FL and FL-Type 2 are based on Table 1 and their membership functions based on Fig. 5, in which the reliability terms are neglected. The rules for FL-PID is based on [16] and Mamdani type inference mechanism and well-known min-max composition and the centroid defuzzification, whereas FL and FL-Type 2 use the Sugeno type fuzzy inference mechanism but FL-Type 2 uses Karnik-Mendel (KM) type reduction [40].

Furthermore, in line with the above motivations, the range of linear velocity is set to [0 m/s, 0.5 m/s], and the range of angular velocity is set to [-6 rpm, 6 rpm], both of which are set equally for Z-FL, FL and FL-Type 2. Following the standard model, FL-PID has no explicit mechanism to ensure fixation of lower and upper bounds on linear and angular velocities. The values of the above velocity boundaries are

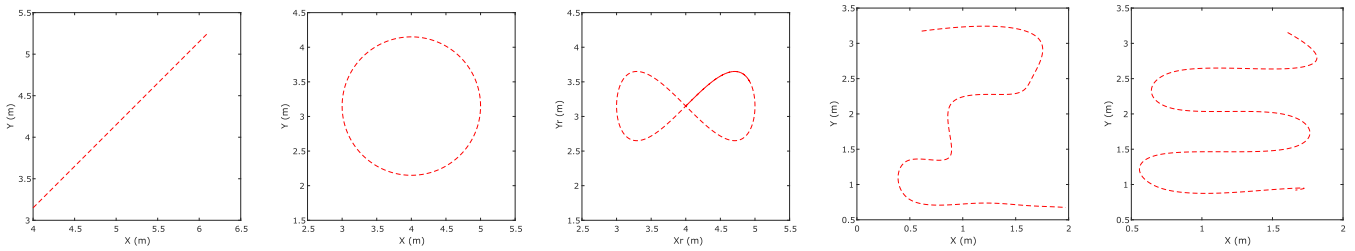

(a) Line (b) Circle (c) Lemniscate (d) B-Spline 1 (e) B-Spline 2

FIGURE 7. Reference scenarios for trajectory tracking include paths with distinct geometry and curvature profiles.

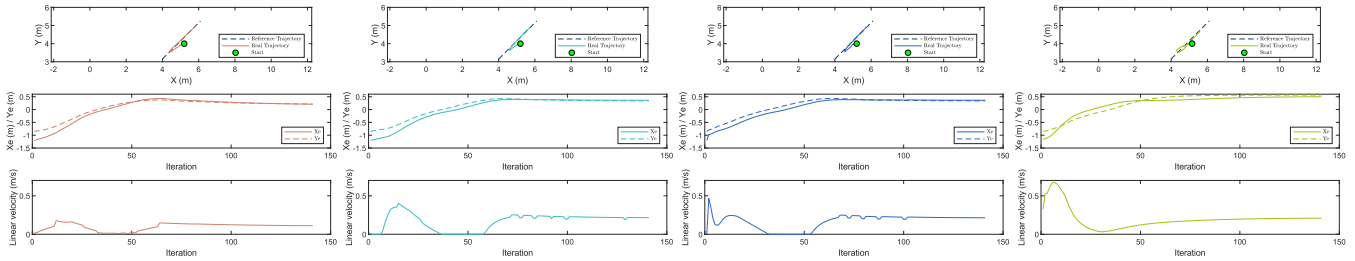

(a) Z-FL (b) FL (c) FL-Type2 (d) FL-PID

FIGURE 8. Results on *line* trajectory tracking. *Top*: Trajectories, *Center*: Error in *X*, *Y* *Bottom*: Linear velocity.

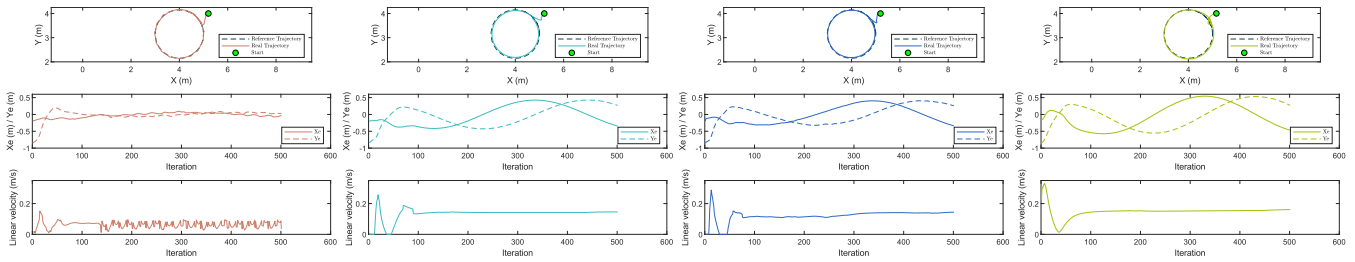

(a) Z-FL (b) FL (c) FL-Type2 (d) FL-PID

FIGURE 9. Results on *circle* trajectory tracking. *Top*: Trajectories, *Center*: Error in *X*, *Y* *Bottom*: Linear velocity.

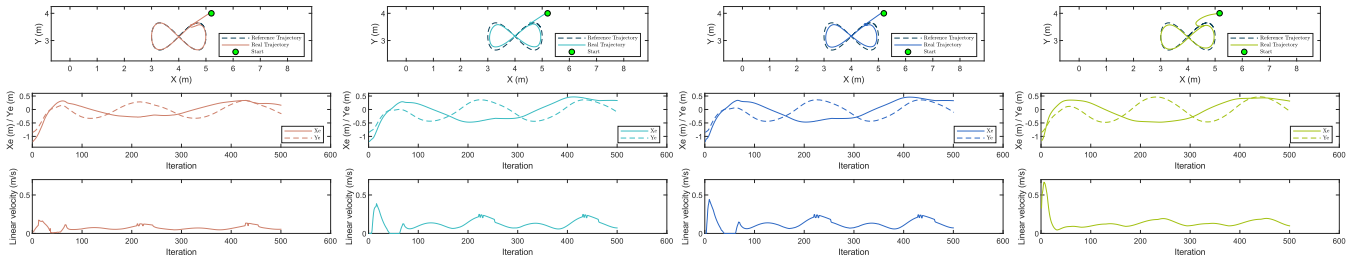

(a) Z-FL (b) FL (c) FL-Type2 (d) FL-PID

FIGURE 10. Results on *lemniscate* trajectory tracking. *Top*: Trajectories, *Center*: Error in *X*, *Y* *Bottom*: Linear velocity.

decided based on our interest and scope to evaluate the suitability for safe navigation at indoor environments. Due to the above fact, the study on the extended upper boundaries of linear and angular velocities (e.g. racing cars) is out of the scope of this paper and is left for future studies in our agenda.

B. TRAJECTORY SCENARIOS

We used trajectory tracking scenarios with distinct curvature profiles to evaluate the performance and generalization ability of Z-FL and the above-described benchmark methods. In particular, we used the following scenarios:

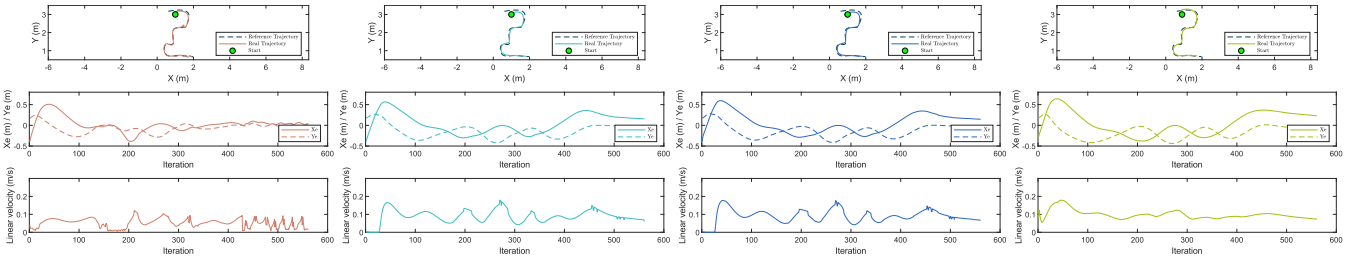

(a) Z-FL (b) FL (c) FL-Type2 (d) FL-PID

FIGURE 11. Results on *B-Spline 1* trajectory tracking. *Top*: Trajectories, *Center*: Error in *X*, *Y Bottom*: Linear velocity.

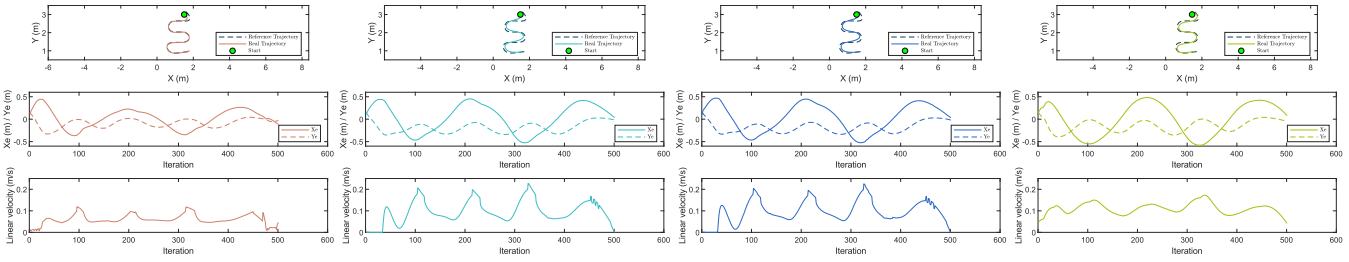

(a) Z-FL (b) FL (c) FL-Type2 (d) FL-PID

FIGURE 12. Results on *B-Spline 2* trajectory tracking. *Top*: Trajectories, *Center*: Error in *X*, *Y Bottom*: Linear velocity.

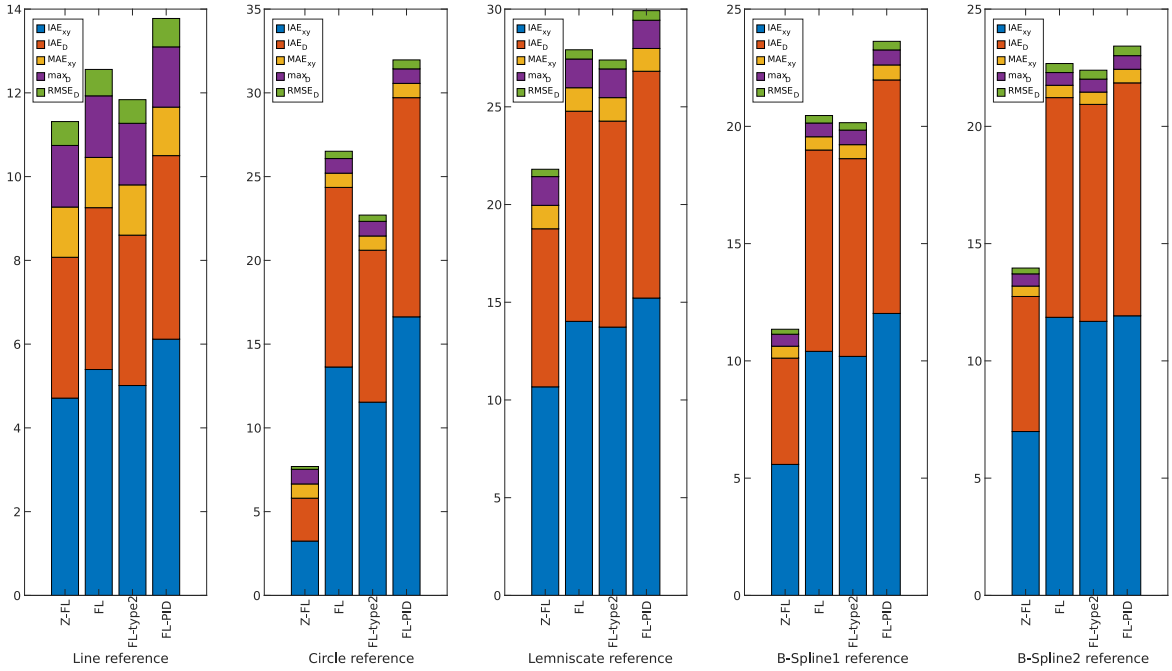

FIGURE 13. Summary of trajectory tracking performance overall scenarios, control methods and performance metrics.

- **Line**. (Fig. 7(a)):

$$(X_r(t), Y_r(t)) = (0.3t + 3.15, 0.3t + 3.15) \quad (23)$$

- **Circle** (Fig. 7(b)):

$$(X_r(t), Y_r(t)) = \Big(cos(0.3t)+4, sin(0.3t)+3.15\Big) \quad (24)$$

- **Lemniscate** (Fig. 7(c)):

$$(X_r(t), Y_r(t)) = \Big(sin(0.3t)+4, sin(0.3t)\cdot cos(0.3t)+3.15\Big) \quad (25)$$

- **B-Spline 1** (Fig. 7(d)):
We generated trajectories by using the versatility of B-Splines to model sophisticated trajectories relevant to

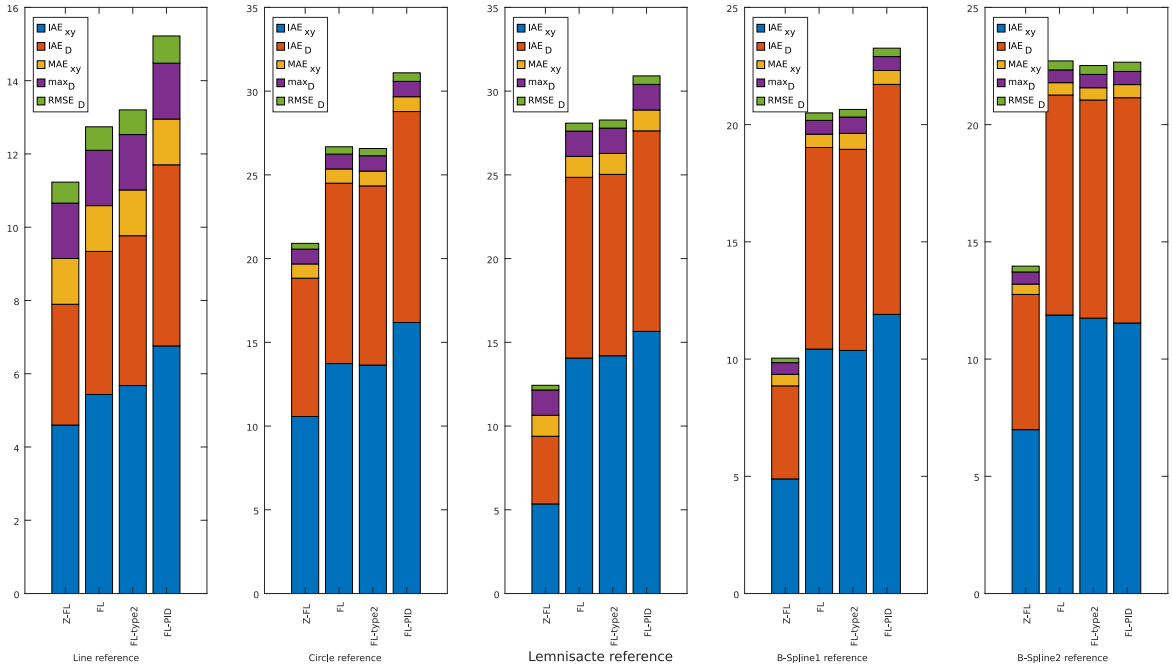

FIGURE 14. Effect of low-level noises in trajectory tracking performance overall scenarios, methods and performance metrics.

real-world applications, as follows:

$$(X_r(t), Y_r(t) = \sum_{c=1}^{NC} \mathcal{B}^{\mathbf{u}}_{c,k}(u) \cdot (\hat{x}_c, \hat{y}_c) \tag{26}$$

$$\mathcal{B}^{\mathbf{u}}_{c,k}(u) = w_{c,k} \cdot \mathcal{B}^{\mathbf{u}}_{c,k-1} + (1 - w_{c+1,k}) \cdot \mathcal{B}^{\mathbf{u}}_{c+1,k-1} \tag{27}$$

$$\mathcal{B}^{\mathbf{u}}_{c,1}(u) = \begin{cases} 1, & \text{if } u \in [u_c, u_{c+1}) \\ 0, & \text{if otherwise} \end{cases} \tag{28}$$

$$w_{c,k}(u) = \begin{cases} \dfrac{u - u_c}{u_{c+k-1} - u_c}, & \text{if } u_c \neq u_{c+k-1} \\ 0, & \text{if otherwise} \end{cases} \tag{29}$$

$$u = u_1 + \frac{t}{T} \cdot (u_L - u_1), \tag{30}$$

where $\mathcal{B}^{\mathbf{u}}_{c,k}$ denotes the B-Spline over the interval $u \in [u_c, u_{c+1})$ with order $k = L - NC$ and knot sequence in non-decreasing order $\mathbf{u} = (u_1, u_2, ..., u_L)$; and $(\hat{x}_c, \hat{y}_c)$ is the cth control point of the above-mentioned B-Spline, $c \in [NC]$, in which $\hat{x}_c$ ($\hat{y}_c$) is the cth element of the tuple $\hat{x}$ ($\hat{y}$), and NC denotes the number of control points.

The reader may note that the above-described trajectory is parameterized over the domain $t \in [0, T]$ and $u \in [u_1, u_L]$, and depends on two factors: the knot sequence $\mathbf{u}$, and the control points $(\hat{x}_c, \hat{y}_c)$, $\forall c \in [NC]$, each of which is user-defined and task-specific.

Thus, by using Eq. 26, the trajectory of B-Spline 1 is defined by the knot sequence $\mathbf{u}$ = (0, 0, 0, 0, 1, 2, 3, 4, 5, 6, 7, 8, 9, 10, 10, 10, 10), and the control points defined by the tuple $\hat{x}$ = (0.61, 1.27, 1.91, 1.62, 1.58, 0.67, 1.07, 0.35, 0.36, 1.17, 1.59, 1.86, 1.97) and the tuple $\hat{y}$ = (3.17, 3.31, 3.17, 2.46, 2.21, 2.38, 1.12, 1.57, 0.60, 0.78, 0.69, 0.69, 0.67). As a result, $L = 17$, $NC = 13$ and $k = 4$.

- **B-Spline2** (Fig. 7(e)):
  By using the same above-described concept (Eq. 26), yet considering a curvature profile with potential application for guided patrol with full coverage, the trajectory of B-Spline 2 is defined by the knot sequence $\mathbf{u}$ = (0, 0, 0, 0, 1, 2, 3, 4, 5, 6, 7, 8, 9, 9, 9, 9), and the control points defined by $\hat{x}$ = (1.61, 1.92, 1.76, 0.60, 0.59, 1.76, 1.87, 0.43, 0.59, 1.54, 1.81, 1.66) and $\hat{y}$ = (3.15, 2.80, 2.53, 2.79, 1.88, 2.19, 1.32, 1.61, 0.77, 0.94, 0.97, 0.92). Here, $L = 16$, $NC = 12$ and $k = 4$.

For all the above-described trajectory scenarios, the parameter t is defined at $0, h, 2h, ..., T$. Here, the following holds: $T = (H - 1)h$, where H is used (1) to define the number of measurements used by the performance metrics outlined by Eq. (18) - Eq. (22), and (2) to quantify the number of control iterations. Due to the distinct geometry of trajectory scenarios, T is set accordingly, i.e. $T = 7$ for the *line* reference (Eq. 23), $T = 25$ for the *circle* (Eq. 24) and the *lemniscate* (25) references, $T = 28$ for *B-Spline 1*, and $T = 25$ for *B-Spline 2*. In line with V-REP configurations, we use $h = 0.05$ for all scenarios and all evaluated methods.

Furthermore, the initial position was set not only to be off-track, but also to have initial heading direction being different from the initial desired direction for navigation. As such, our aim is to evaluate the above-described trajectory tracking methods under challenging conditions. Due to the combination nature of all possible robot configurations in the plane, it is computationally intractable to evaluate all such

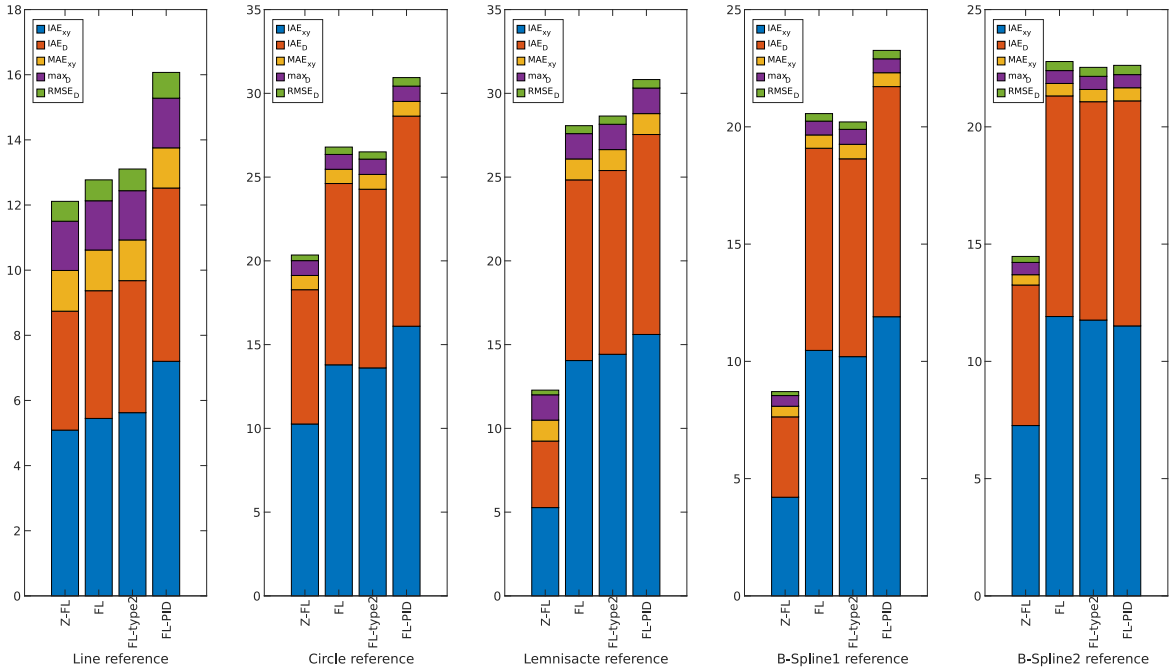

FIGURE 15. Effect of *high*-level noises in trajectory tracking performance overall scenarios, methods and performance metrics.

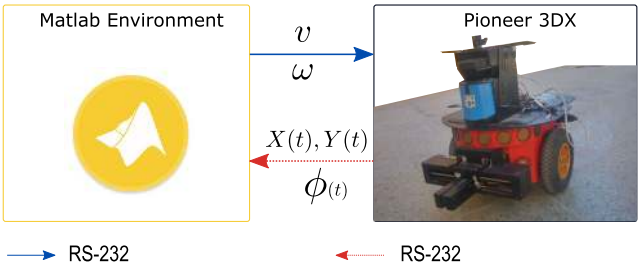

FIGURE 16. Interface of Pioneer P3-DX mobile robot.

configurations. Yet, we believe that the above notion is relevant to better grasp the performance of trajectory tracking for mobile robots. Thus, under the above-mentioned motivations, the initial robot position was set to (5.25 m, 4 m, $-\pi$ rad) for the line, the circle and the lemniscate scenarios; and (1 m, 3 m, $-\pi$ rad) and (1.5 m, 3 m, $-\pi$ rad), for the B-Spline 1 and B-Spline 2 scenarios, respectively.

C. RESULTS AND ANALYSIS

In order to show the performance of trajectory tracking of Z-FL and the related approaches, Figs 8-12 show the reference and achieved trajectory (top), the error of both x-axis and y-axis (middle), and the achieved linear velocity (bottom). Also, Fig. 13 shows the accuracy metrics of Z-FL and the related approaches in terms of IAE_{xy} (blue), IAE_D (orange), MAE_{xy} (yellow), max(D) (purple) and $RMSE_D$ (green). By observing these figures, we note the following facts:

- In line and circle trajectories, Z-FL is significantly better in terms of IAE_{xy} and IAE_D.
- There is no significant difference among Z-FL, FL, FL-type2 in terms of MAE_{xy} and $\max_D$ at line, circle and lemniscate trajectories.
- In lemniscate trajectory, FL-PID is better than Z-FL in terms of MAE_{xy} and $\max_D$, however Z-FL is significantly better in terms of IAE_{xy}, IAE_D and $RMSE_D$.
- In circle, lemniscate and B-spline 2 trajectories, Z-FL is significantly better than other controllers regarding minimum overshoot and steady state error of $X(t)$ and $Y(t)$ displacement errors.
- In all trajectories, although the average speed of Z-FL is lower than other controllers, the fluctuation amplitude is comparatively smaller than other controllers, implying the improved comfortability.

Overall, Z-FL achieves significantly better trajectory tracking performance compared to the related approaches. We believe the above results are due to not only the representation of uncertainty in Z-FL, but also due to the interpolation and the inference system. Encoding the reliability in the input allows to extend the versatility (degrees of freedom) of the control landscape, the interpolative reasoning allows tackling missing observations in the rule base, and the inference system allows to preserve ambiguity when computing with Z-numbers.

D. EFFECT OF NOISE

To evaluate the robustness of the proposed Z-FL controller, we performed rigorous computational experiments by adding arbitrary Gaussian noise as follows: $\omega_{r(l)} = \omega_{r(l)} + \delta \cdot p$, where $p \in \mathcal{N}(0, 1)$ is a random number with standard normal distribution, and $\delta = 0.1(1)$ is termed as low (high)

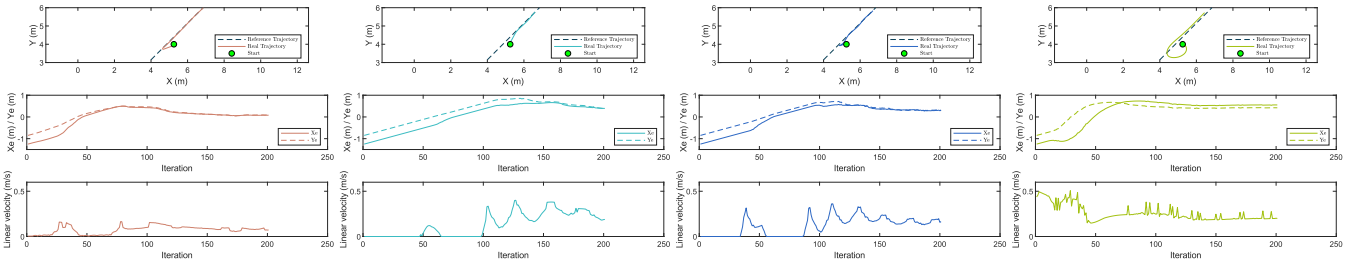

(a) Z-FL (b) FL (c) FL-Type2 (d) FL-PID

FIGURE 17. ***Line*** **trajectory tracking using a Pioneer 3DX robot.** ***Top*****: Trajectories,** ***Center*****: Error in** ***X*** **,** ***Y*** **Bottom: Linear velocity.**

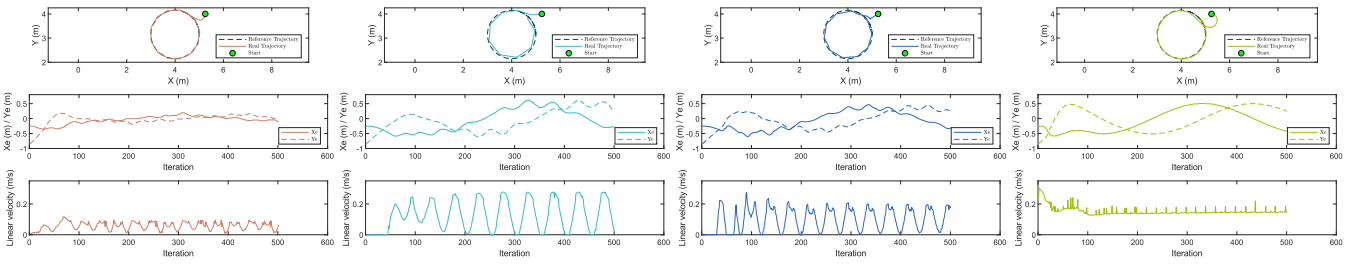

(a) Z-FL (b) FL (c) FL-Type2 (d) FL-PID

FIGURE 18. ***Circle*** **trajectory tracking using a Pioneer 3DX robot.** ***Top*****: Trajectories,** ***Center*****: Error in** ***X*** **,** ***Y*** **Bottom: Linear velocity.**

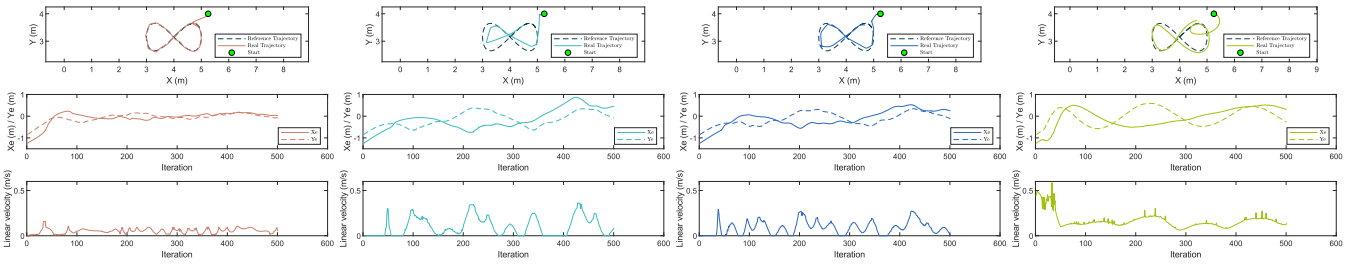

(a) Z-FL (b) FL (c) FL-Type2 (d) FL-PID

FIGURE 19. ***Lemniscate*** **trajectory tracking using a Pioneer 3DX robot.** ***Top*****: Trajectories,** ***Center*****: Error in** ***X*** **,** ***Y*** **Bottom: Linear velocity.**

noise. The simulation time is divided into three phases: in the first/second/third phase, noise is added to the angular velocity of the right/left/both wheel(s).

To show the robustness performance under noise inducements, Figs. 14 and 15 show the accuracy metrics of all approaches in terms of IAE_{xy} (blue), IAE_D (orange), MAE_{xy} (yellow), max(D) (purple) and $RMSE_D$ (green). As we can observe, Z-FL shows the comparatively better performance on all trajectories with high and low noise level, except w.r.t MAE_{xy} under high-noise level. We believe these results are in line with ability of Z-FL to cope with missing observations and the efficiency (and better response to noise) when handling ambiguity.

V. EXPERIMENTAL STUDIES

In order to evaluate the performance of Z-FL and the related approaches on a real-world scenario relevant to trajectory tracking, we used a Pioneer 3DX mobile robot (see Fig. 16) embedded with an onboard laptop. In all the real-world experiments, we used MATLAB 2019a, and the same trajectory (noise) configurations outlined in Sec. 4.2 (Sec. 4.4). As such, we carried out 60 experiments (4 trajectory tracking methods, 5 path tracking scenarios, 3 situations considering noises on wheel speed).

The computing environment in our laptop was an Intel(R)Core(TM) i5-6200 CPU @2.3GHz, 8 GB RAM, 2 cores and Windows 10, 64 bit. The laptop communicated with the robot through an RS-232 compatible serial port, and a client-server interface based on the Advanced Robotics Control and Operations Software (ARCOS) [41]. Communication with the Pioneer 3DX robot was realized with one second sample time. Also, the initial angle is set to 0 rad to allow the challenging path tracking scenario since the initial pose is opposite to the tracked path. The main parameters of Pioneer 3DX are as follows: $L = 39\ cm$, $r_w = 10\ cm$, all of which denote the reported hardware configurations [42].

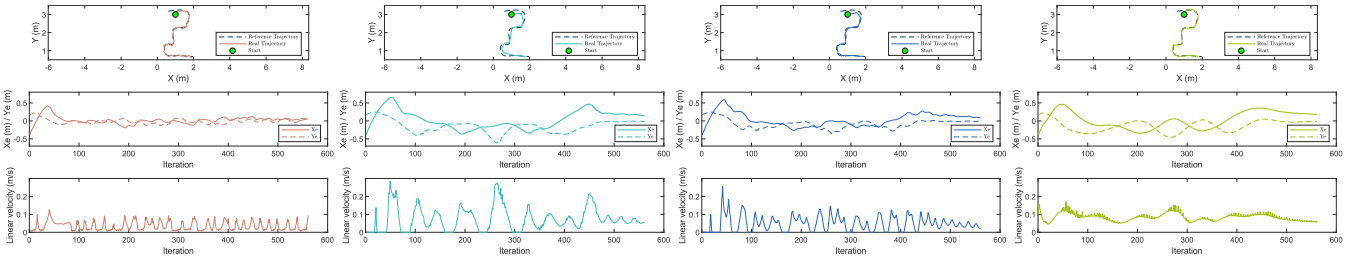

(a) Z-FL (b) FL (c) FL-Type2 (d) FL-PID

FIGURE 20. ***B-Spline 1*** **trajectory tracking using a Pioneer 3DX robot.** ***Top*****: Trajectories,** ***Center*****: Error in** ***X*****,** ***Y*** ***Bottom*****: Linear velocity.**

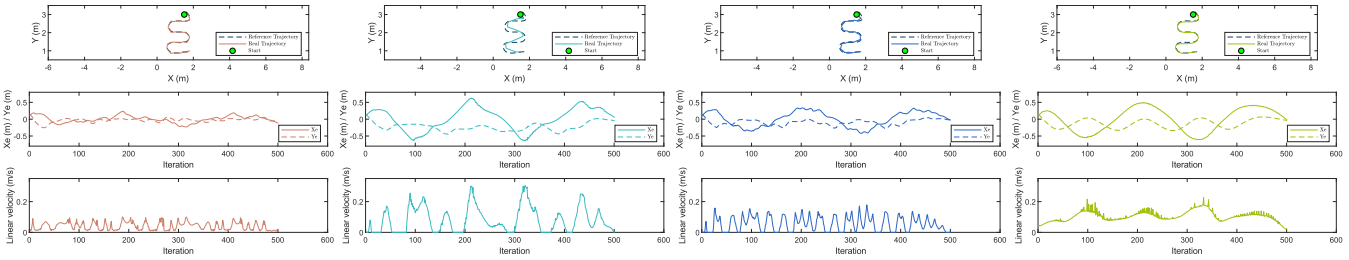

(a) Z-FL (b) FL (c) FL-Type2 (d) FL-PID

FIGURE 21. ***B-Spline 2*** **trajectory tracking using a Pioneer 3DX robot.** ***Top*****: Trajectories,** ***Center*****: Error in** ***X*****,** ***Y*** ***Bottom*****: Linear velocity.**

In order to show the performance of trajectory tracking of Z-FL and the related approaches, Fig. 17-21 show the reference and achieved trajectory (top), the error of both x-axis and y-axis (middle), and the achieved linear velocity (bottom). Also, Fig. 22 shows the summary of accuracy metrics of Z-FL and the related approaches in terms of IAE_{xy} (blue), IAE_D (orange), MAE_{xy} (yellow), max(D) (purple) and $RMSE_D$ (green). As we can observe from Figs. 17 - 22 we can note the following facts:

- Overall trajectories, Z-FL is significantly better than all related algorithms.
- There is no significant difference among controllers in terms of max_D and MAE_{xy} at line, circle and lemniscate trajectories.
- In all trajectories, Z-FL is significantly better than other controllers regarding minimum overshoot and steady state error of $X(t)$ and $Y(t)$ displacement errors.
- The smooth paths are obtained by both FL-PID and Z-FL.

By considering the above facts, Z-FL is shown to be comparatively superior to other relevant approaches in real-world experiments, in which real trajectories are followed with minimal errors.

A. EFFECT OF NOISE

To evaluate the robustness of Z-FL and of the related approaches, we performed rigorous real-world experiments by adding arbitrary Gaussian noises to the robot velocities (linear and angular velocities), following the same notions outlined in Sec. 4.4.

In order to show the comparison of robustness on trajectory tracking of Z-FL and the related approaches, Fig. 23 and Fig. 24 show the summary of accuracy metrics of Z-FL and the related approaches in terms of IAE_{xy} (blue), IAE_D (orange), MAE_{xy} (yellow), max(D) (purple) and $RMSE_D$ (green). From these figures, we note the following facts:

- In all trajectories with *high* and *low* level of noise, Z-FL is significantly better than other controllers.
- There is no significant difference among controllers in terms of $\max_D$ and MAE_{xy} at line, circle and lemniscate trajectories.

Furthermore, the previous results allow identifying a number of insights:

- In all scenarios, Z-FL outperforms other controllers on IAE_{xy} and IAE_D, implying Z-FL demonstrates the unique advantage of minimizing the error over a sustained period of time.
- In all scenarios, Z-FL outperforms other controllers on $RMSE_D$ which implies Z-FL is able to eliminate small and large errors.
- Z-FL has the minimum MAE_{xy} and $\max_D$ in most of scenarios which implies that Z-FL is suitable for narrow environments.
- Z-FL shows the utmost attractive performance from the viewpoint of accuracy under diverse levels of noise., implying the improved level of robustness.
- In all trajectories, although the average speed of the robot using Z-FL is slower than other controllers, the fluctuation amplitude is smaller compared to other

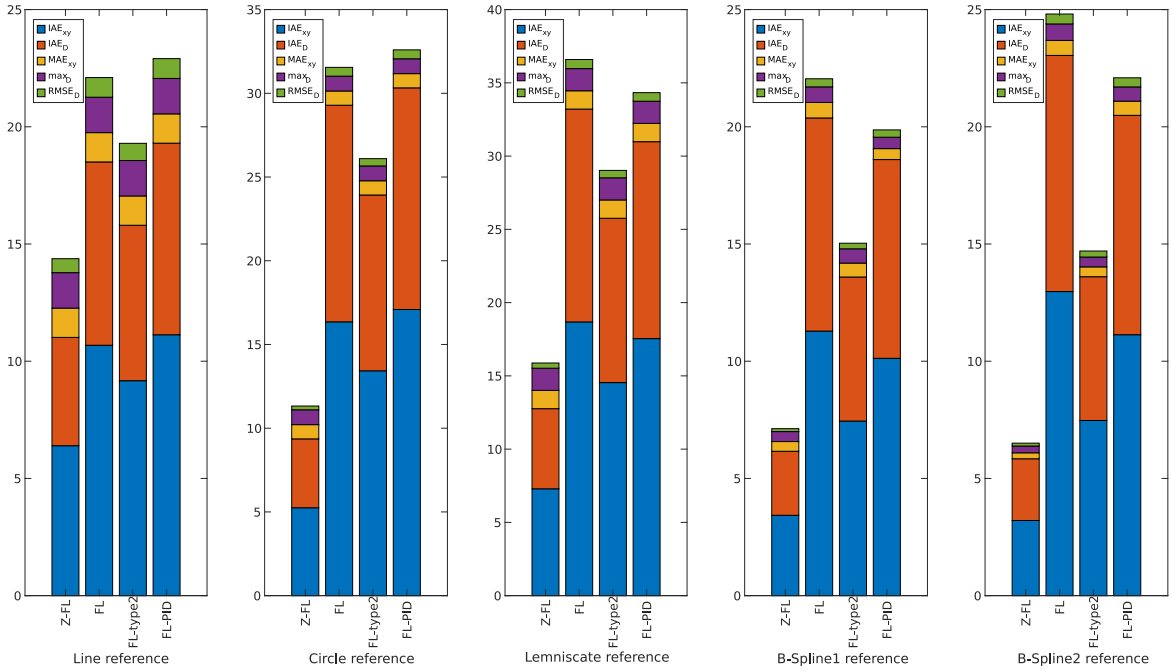

FIGURE 22. Summary of trajectory tracking real performance overall scenarios and performance metrics.

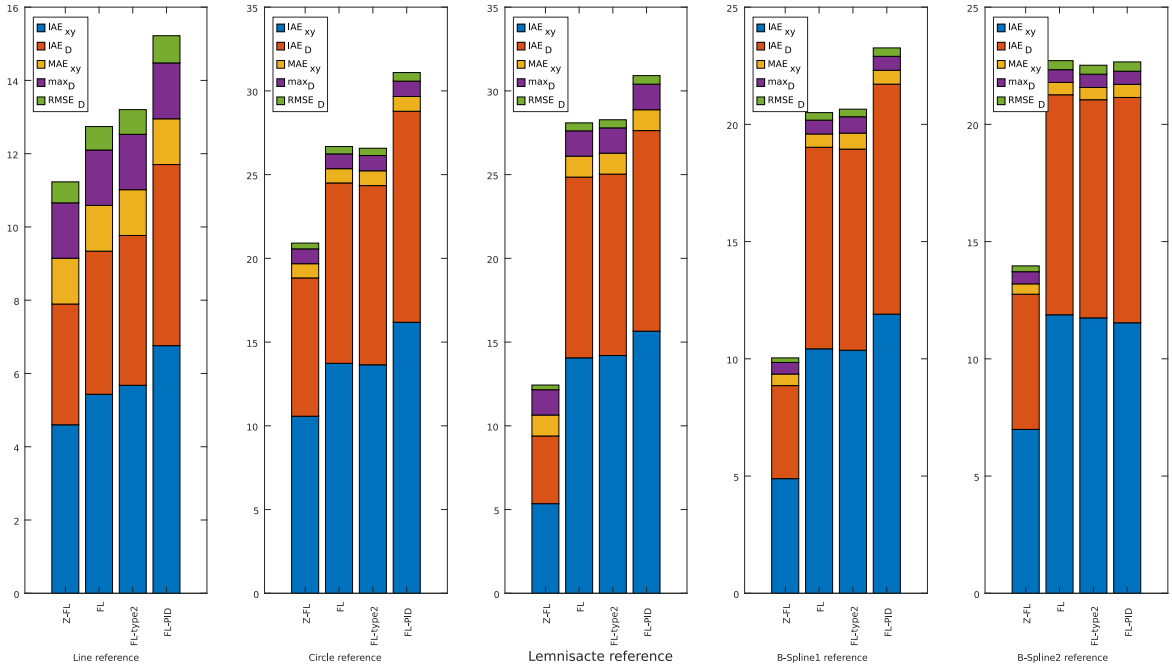

FIGURE 23. Summary of trajectory tracking real performance overall scenarios and performance metrics under *low*-level noise inducements.

controllers, which implies the improved driving comfortability.

Considering the performance on both simulation and real-world tests, Z-FL attained the utmost overall performance on the studied trajectory tracking scenarios; implying that Z-FL is advantageous for trajectory tracking especially at moderate speeds, e.g. navigation in indoor environments such as factories and hospitals needing safe navigation with moderate speed. In future work, we aim at addressing the trajectory tracking problem at higher speeds by using the appropriate robot hardware and interface allowing the navigation in indoor and outdoor environments relevant for fast patrolling, road planning and exploration.

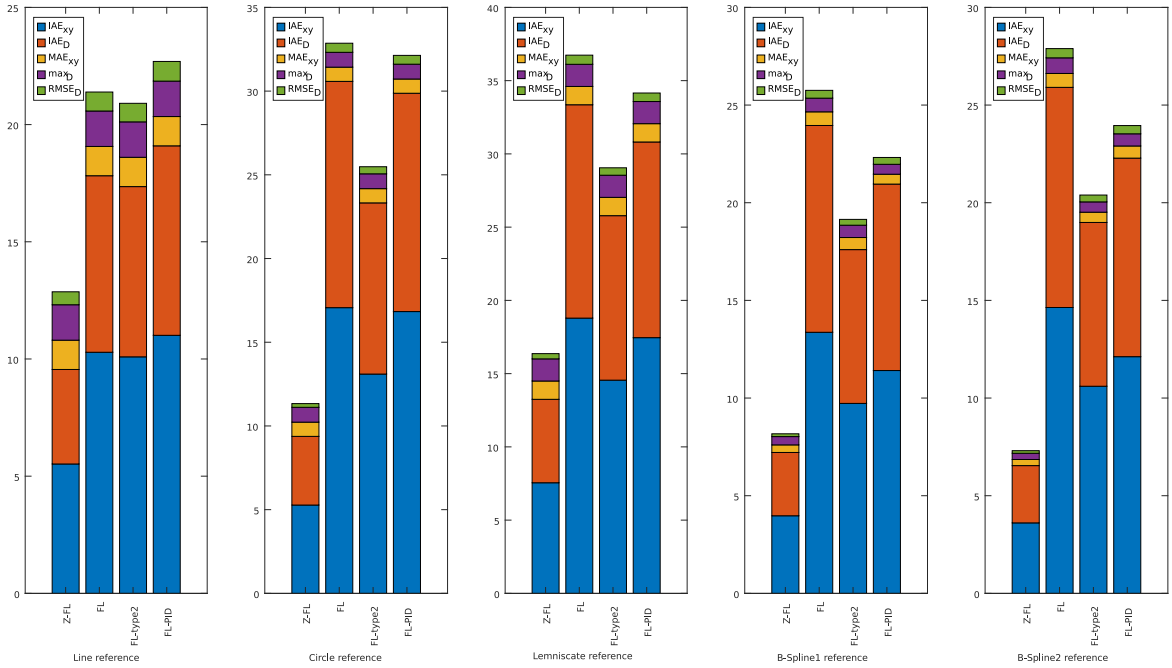

FIGURE 24. Summary of trajectory tracking real performance overall scenarios and performance metrics under ***high*-level noise inducements.**

VI. CONCLUSION

We presented a Z-number based Fuzzy Logic (Z-FL) control scheme for trajectory tracking with rules encodes by the instantaneous measurements of both the (Euclidean) distance to target and the orientation gap. Not only our approach avoids the complexity of encoding the gradient of the tracking errors, but also it is more amenable to model the multi-input-multi-output nature of mobile robots, therefore allowing finer expressibility of the non-linear control landscapes, and better ability to evaluate the performance at high resolutions; all of which is relevant for practical navigation scenarios.

Our in-depth and rigorous scrutiny using both simulations and real-world experiments based on the Pioneer 3DX mobile robot elucidated the outstanding effectiveness and the feasibility of Z-FL in terms of accuracy, robustness and velocity fluctuation compared to the related controllers such as Fuzzy Logic, Fuzzy Logic Type 2 and Fuzzy Logic-PID for trajectory tracking in navigation scenarios with a relevant set of curvature profiles.

Our results provide the state-of-the-art insights useful to realize control algorithms aided by FL and Z-number, able to achieve robust and generalizable performance. Our future works involve developing higher-order interpolation methods enabling tracking at higher speeds and robust performance.

REFERENCES

[1] S. S. H. Hajjaj and K. S. M. Sahari, "Review of research in the area of agriculture mobile robots," in *Proc. 8th Int. Conf. Robot., Vis., Signal Process. Power Appl.* Singapore: Springer, 2014, pp. 107–117.

[2] G. Bai, L. Liu, Y. Meng, W. Luo, Q. Gu, and J. Wang, "Path tracking of wheeled mobile robots based on dynamic prediction model," *IEEE Access*, vol. 7, pp. 39690–39701, 2019.

[3] R. Wallace, A. Stentz, C. Thorpe, H. Maravec, W. Whittaker, and T. Kanade, "First results in robot road-following," in *Proc. 9th Int. Joint Conf. Artif. Intell. (IJCAI)*, vol. 2, 1985, pp. 1089–1095.

[4] M. Samuel, M. Hussein, and M. Binti, "A review of some pure-pursuit based path tracking techniques for control of autonomous vehicle," *Int. J. Comput. Appl.*, vol. 135, no. 1, pp. 35–38, Feb. 2016.

[5] P. Zhao, J. Chen, Y. Song, X. Tao, T. Xu, and T. Mei, "Design of a control system for an autonomous vehicle based on adaptive-PID," *Int. J. Adv. Robot. Syst.*, vol. 9, no. 2, p. 44, Aug. 2012.

[6] E. Kayacan and G. Chowdhary, "Tracking error learning control for precise mobile robot path tracking in outdoor environment," *J. Intell. Robot. Syst.*, vol. 95, nos. 3–4, pp. 975–986, Sep. 2019.

[7] C. Wang, X. Liu, X. Yang, F. Hu, A. Jiang, and C. Yang, "Trajectory tracking of an Omni-directional wheeled mobile robot using a model predictive control strategy," *Appl. Sci.*, vol. 8, no. 2, p. 231, Feb. 2018.

[8] J. Cai, H. Jiang, L. Chen, J. Liu, Y. Cai, and J. Wang, "Implementation and development of a trajectory tracking control system for intelligent vehicle," *J. Intell. Robot. Syst.*, vol. 94, no. 1, pp. 251–264, Apr. 2019.

[9] I. Zohar, A. Ailon, and R. Rabinovici, "Mobile robot characterized by dynamic and kinematic equations and actuator dynamics: Trajectory tracking and related application," *Robot. Auton. Syst.*, vol. 59, no. 6, pp. 343–353, Jun. 2011.

[10] J.-Y. Zhai and Z.-B. Song, "Adaptive sliding mode trajectory tracking control for wheeled mobile robots," *Int. J. Control*, vol. 92, no. 10, pp. 2255–2262, Oct. 2019.

[11] M. Asif, A. Y. Memon, and M. J. Khan, "Output feedback control for trajectory tracking of wheeled mobile robot," *Intell. Autom. Soft Comput.*, vol. 22, no. 1, pp. 75–87, Jan. 2016.

[12] M. M. Michałek and T. Gawron, "VFO path following control with guarantees of positionally constrained transients for unicycle-like robots with constrained control input," *J. Intell. Robot. Syst.*, vol. 89, nos. 1–2, pp. 191–210, Jan. 2018.

[13] C. Ren and S. Ma, "Trajectory tracking control of an omnidirectional mobile robot with friction compensation," in *Proc. IEEE/RSJ Int. Conf. Intell. Robots Syst. (IROS)*, Oct. 2016, pp. 5361–5366.

[14] G. Huskic, S. Buck, and A. Zell, "Path following control of skid-steered wheeled mobile robots at higher speeds on different terrain types," in *Proc. IEEE Int. Conf. Robot. Autom. (ICRA)*, May 2017, pp. 3734–3739.

[15] M. Deremetz, R. Lenain, and B. Thuilot, "Path tracking of a two-wheel steering mobile robot: An accurate and robust multi-model off-road steering strategy," in *Proc. IEEE Int. Conf. Robot. Autom. (ICRA)*, May 2018, pp. 3037–3044.
[16] D. K. Tiep, K. Lee, D.-Y. Im, B. Kwak, and Y.-J. Ryoo, "Design of fuzzy-PID controller for path tracking of mobile robot with differential drive," *Int. J. Fuzzy Logic Intell. Syst.*, vol. 18, no. 3, pp. 220–228, Sep. 2018.
[17] Q. Xu, J. Kan, S. Chen, and S. Yan, "Fuzzy PID based trajectory tracking control of mobile robot and its simulation in simulink," *Int. J. Control Automat.*, vol. 7, no. 8, pp. 233–244, Aug. 2014.
[18] X. Wu, P. Jin, T. Zou, Z. Qi, H. Xiao, and P. Lou, "Backstepping trajectory tracking based on fuzzy sliding mode control for differential mobile robots," *J. Intell. Robot. Syst.*, vol. 96, no. 1, pp. 109–121, Oct. 2019.
[19] S. Cho, B. Shrestha, W. Jang, and C. Seo, "Trajectory tracking optimization of mobile robot using artificial immune system," *Multimedia Tools Appl.*, vol. 78, no. 3, pp. 3203–3220, Feb. 2019.
[20] S. Dian, J. Han, R. Guo, S. Li, T. Zhao, Y. Hu, and Q. Wu, "Double closed-loop general type-2 fuzzy sliding model control for trajectory tracking of wheeled mobile robots," *Int. J. Fuzzy Syst.*, vol. 21, no. 7, pp. 2032–2042, Oct. 2019.
[21] H.-M. Wu and M. Karkoub, "Hierarchical fuzzy sliding-mode adaptive control for the trajectory tracking of differential-driven mobile robots," *Int. J. Fuzzy Syst.*, vol. 21, no. 1, pp. 33–49, Feb. 2019.
[22] L. A. Zadeh, "A note on Z-numbers," *Inf. Sci.*, vol. 181, no. 14, pp. 2923–2932, 2011.
[23] R. R. Yager, "On a view of Zadeh's Z-numbers," in *Advances in Computational Intelligence*, S. Greco, B. Bouchon-Meunier, G. Coletti, M. Fedrizzi, B. Matarazzo, and R. R. Yager, Eds. Berlin, Germany: Springer, 2012, pp. 90–101, doi: 10.1007/978-3-642-31718-7_10.
[24] R. R. Yager, "On Z-valuations using Zadeh's Z-numbers," *Int. J. Intell. Syst.*, vol. 27, no. 3, pp. 259–278, Mar. 2012.
[25] R. H. Abiyev, "Z number based fuzzy inference system for dynamic plant control," *Adv. Fuzzy Syst.*, vol. 2016, pp. 1–7, Nov. 2016.
[26] R. A. Aliev, W. Pedrycz, O. H. Huseynov, and S. Z. Eyupoglu, "Approximate reasoning on a basis of Z-number-valued if-then rules," *IEEE Trans. Fuzzy Syst.*, vol. 25, no. 6, pp. 1589–1600, 2017.
[27] R. Aliev and K. Memmedova, "Application of Z-number based modeling in psychological research," *Comput. Intell. Neurosci.*, vol. 2015, p. 11, Jan. 2015.
[28] R. A. Aliev, W. Pedrycz, A. V. Alizadeh, and O. H. Huseynov, "Fuzzy optimality based decision making under imperfect information without utility," *Fuzzy Optim. Decis. Making*, vol. 12, no. 4, pp. 357–372, Dec. 2013.
[29] B. Kang, D. Wei, Y. Li, and Y. Deng, "A method of converting Z-number to classical fuzzy number," *J. Inf. Comput. Sci.*, vol. 9, no. 3, p. 703, 2012.
[30] R. H. Abiyev, N. Akkaya, and I. Gunsel, "Control of omnidirectional robot using Z-number-based fuzzy system," *IEEE Trans. Syst., Man, Cybern., Syst.*, vol. 49, no. 1, pp. 238–252, Jan. 2019.
[31] L. T. Kóczy and K. Hirota, "Interpolative reasoning with insufficient evidence in sparse fuzzy rule bases," *Inf. Sci.*, vol. 71, nos. 1–2, pp. 169–201, Jun. 1993.
[32] C.-C. Chou, "The canonical representation of multiplication operation on triangular fuzzy numbers," *Comput. Math. Appl.*, vol. 45, nos. 10–11, pp. 1601–1610, May 2003.
[33] M. Abdelwhab, A. A. Abouelsoud, and A. M. R. F. Elbab, "Tackling dead end scenarios by improving follow gap method with genetic programming," in *Proc. 57th Annu. Conf. Soc. Instrum. Control Eng. Jpn. (SICE)*, Sep. 2018, pp. 1566–1571.
[34] M. Alzubi, Z. C. Johanyák, and S. Kovács, "Fuzzy rule interpolation methods and fri toolbox," *CoRR*, vol. 96, no. 21, pp. 7227–7244, Apr. 2019.
[35] S. Chen and C. Hsieh, "Graded mean integration representation of generalized fuzzy number," in *Proc. 6th Conf. Fuzzy Theory Appl.*, 1998, pp. 1–6.
[36] M. Delgado, M. Vila, and W. Voxman, "On a canonical representation of fuzzy numbers," *Fuzzy Sets Syst.*, vol. 93, no. 1, pp. 125–135, Jan. 1998.
[37] Y. Deng, Y. Chen, Y. Zhang, and S. Mahadevan, "Fuzzy Dijkstra algorithm for shortest path problem under uncertain environment," *Appl. Soft Comput.*, vol. 12, no. 3, pp. 1231–1237, Mar. 2012.
[38] D. Hazry and M. Sugisaka, "Proportional control for trajectory tracking of a wheeled mobile robot," in *Proc. SICE-ICASE Int. Joint Conf.*, Oct. 2006, pp. 5283–5285.
[39] M. R. H. Al-Dahhan and M. M. Ali, "Path tracking control of a mobile robot using fuzzy logic," in *Proc. 13th Int. Multi-Conf. Syst., Signals Devices (SSD)*, Mar. 2016, pp. 82–88.
[40] A. Taskin and T. Kumbasar, "An open source MATLAB/simulink toolbox for interval type-2 fuzzy logic systems," in *Proc. IEEE Symp. Ser. Comput. Intell.*, Dec. 2015.
[41] J. Calusdian and X. Yun, "A simple and highly portable MATLAB interface for learning robotics," *SN Appl. Sci.*, vol. 1, no. 8, p. 890, Jul. 2019.
[42] (2006). *Pioneer 3 Operations Manual*. [Online]. Available: https://www.generationrobots.com/en/402395-robot-mobile-pioneer-3-dx.html

MOHAMED ABDELWAHAB (Member, IEEE) received the B.Sc. and M.Sc. degrees in mechanical engineering and automotive section from Ain Shams University, Cairo, Egypt, in 2010 and 2015, respectively, and the Ph.D. degree in the robotics and mechatronics system design from the Egypt-Japan University of Science and Technology, E-JUST, and is a Teaching Assistant with the Department of Automotive Engineering, Ain Shams University. He is an advisor of the Team of Formula Student (FS) from Ain Shams University, planning to participate in FS 2020 UK, and Eco-Shell Marathon. He has participated in designing and manufacturing golf cars with aluminium chassis in Egypt which are working now in Cairo airport. His current research interests include control of wheeled mobile robots, path planning, and tracking in the unstructured environment.

VICTOR PARQUE (Member, IEEE) received the B.Sc. degree in systems engineering from National Central University, in 2004, the MBA degree from the Graduate School of Business Administration, Esan University, in 2009, and the Ph.D. degree from the Graduate School of Information, Production and Systems, Waseda University, in 2011. He was a Postdoctoral Fellow at the Department of Mechanical Engineering, Toyota Technological Institute, from 2012 to 2014, and an Assistant Professor at Waseda University, from 2014 to 2018. He is currently an Associate Professor with the Department of Modern Mechanical Engineering, Waseda University, as well as the JSUC Tokunin Professor at the Egypt-Japan University of Science and Technology. He is the first author of more than 70 articles in journals, conferences, and book chapters, and is actively involved in research collaborations with both industry and academia. His research interests span the principles of learning and intelligent systems and its applications to design engineering, planning, and control. He is a member of the IEEE (RAS, IES, SMC), ACM (SIGAI, SIGEVO), the Robotics Society of Japan (RSJ), and the Japan Society for Precision Engineering (JSPE). He was honoured as a finalist in the Hummies Awards for Human-Competitive Results, in 2018.

AHMED M. R. FATH ELBAB was born in Cairo, Egypt, in 1974. He received the M.Sc. and Ph.D. degrees from Assiut University, Assiut, Egypt, in 2002 and 2008, respectively. His Ph.D. work was in the field of micromachined tactile sensors for robotics and medical applications. From October 2006 to October 2008, he was a Visiting Researcher at Tabata Laboratory, Kyoto University, Kyoto, Japan. During this period, he gained experience in microfabrication experimentally. Since January 2009, he has been a Lecturer (Assistant Professor) with the Department of Mechanical Engineering, Faculty of Engineering, Assiut University, and then became an Associate Professor, in December 2014. He is currently the Department Head of the Mechatronics and Robotics Engineering Department, Egypt-Japan University of Science and Technology, Alexandria, Egypt. His current interests include microsensors (principle, simulation, design, and fabrication), micromachining and its application in MEMS, tactile sensing systems (tactile sensing and display), micro energy harvesting devices, and microfluidics systems. He was a recipient of the Best Ph.D. Thesis Prize in Engineering Sciences from Assiut University, in 2010.

A. A. ABOUELSOUD received the B.Sc. degree (Hons.) in electronics and communications engineering, the M.Sc. degree in control engineering, and the Ph.D. degree in control engineering from Cairo University, Egypt, in 1986, 1989, and 1995. He was a Visiting Assistant Professor at Washington State University, WA, USA, in 2001. He joined Sultan Qaboos University, Oman, from 2008 to 2009, and Taibah University, Saudi Arabia, from 2011 to 2012, respectively. He joined the Egypt-Japan University of Science and Technology, E-JUST, from 2013 to 2018. He works as a part-time External Moderator with the Jomo Kenyatta University for Agriculture and Technology, Kenya, for the undergraduate and postgraduate programs of mechatronics engineering. He is currently a Professor of automatic control with the Electronics and Communications Engineering Department, Cairo University. He has published more than 40 journal and 30 conference papers in automatic control, and robotics. His research interests are in nonlinear and adaptive control, process control, and distributed control systems.

SHIGEKI SUGANO (Fellow, IEEE) received the B.S., M.S., and Dr. Eng. degrees in mechanical engineering from Waseda University, Shinjuku, Japan, in 1981, 1983, and 1989, respectively. From 1986 to 1990, he was a Research Associate at Waseda University. Since 1990, he has been a Faculty Member of the Department of Mechanical Engineering, Waseda University, where he is currently a Professor. From 1993 to 1994, he was a Visiting Scholar with the Mechanical Engineering Department, Stanford University, Stanford, CA, USA. He is a member of the Humanoid Robotics Institute, Waseda University, where he has been the Dean of the School of Creative Science and Engineering, since 2014. Since 2013, he has been serving as the Program Coordinator of the MEXT Leading Graduate Program: Waseda Embodiment Informatics Program. He is currently a Professor with the Department of Modern Mechanical Engineering, Waseda University. His current research interests include human-symbiotic anthropomorphic robot design, dexterous and safety manipulator, and human-robot communication. From 2001 to 2010, he was the President of the Japan Association for Automation Advancement. In 2017, he has served as the President of SICE. He is a Fellow Member of the JSME, SICE, and RSJ, as well as a member of the ASME. Besides his activities as the General Co-Chair of IROS2006, ICRA2012, he has served as the General Chair of the IROS2013 in Tokyo and the SICE Annual Conference 2011.